High-frequency study of nonequilibrium transport in heterostructure bipolar transistors

Y. K. Chen, A. F. J. Levi, R. N. Nottenburg, P. H. Beton,[a] and M. B. Panish
AT&T Bell Laboratories, 600 Mountain Avenue, Murray Hill, New Jersey 07974

(Received 9 June 1989; accepted for publication 21 August 1989)

We report results of studying nonequilibrium transport in heterostructure bipolar transistors at a millimeter-wave band. Increasing the total potential drop in the collector from 0.88 to 1.6 eV changes the measured intrinsic transit delay from 0.32 to 0.63 ps due to the increasing importance of intervalley scattering. Both the experimental and calculated data illustrate the role nonequilibrium transport and intervalley scattering have in determining the fundamental limits to device performance.

The ultimate speed of a bipolar transistor is determined by electron transit time through the base τ_b and the collector τ_c. Reducing the vertical dimensions of the base and collector reduces this time, $\tau_F = \tau_b + \tau_c$. In the past, hot-electron spectroscopy has been used to study nonequilibrium electron distribution functions in heterostructure bipolar transistors (HBTs) (Ref. 1). However, until now, the dynamics of electron transport in such devices have not been directly measured. For the first time, we report results of measuring the intrinsic transit time of nonequilibrium carriers in subpicosecond HBTs. Numerical simulations, which include a detailed description of carrier scattering mechanisms in these devices, confirm the dominant role nonequilibrium carrier transport has in determining high-speed performance.

A schematic band diagram of an InP/$In_{0.53}Ga_{0.47}As$ HBT is shown in Fig. 1. As illustrated in the figure, the transistor operates by injecting a nonequilibrium distribution of electrons with excess kinetic energy, $E = 300$ meV, into the base. The devices used in our experiments have a base thickness $Z_b = 500$ Å, collector thickness $Z_c = 3000$ Å, and are similar to those previously reported in Ref. 2. The wide band-gap n-type InP emitter has an area $2.5 \times 11\ \mu m^2$, p-type doping in the $In_{0.53}Ga_{0.47}As$ base is $1 \times 10^{20}\ cm^{-3}$, the $In_{0.53}Ga_{0.47}As$ collector is doped n type to $3 \times 10^{16}\ cm^{-3}$, and the subcollector is heavily doped n type $5 \times 10^{19}\ cm^{-3}$. The total potential across the collector depletion region is ϕ_{BC}. Small-signal s parameters were measured from 1 to 40 GHz using a pair of millimeter-wave wafer probes and an HP8510B vector network analyzer. It is essential to perform these measurements with the sample maintained at a temperature of 80 K so that intrinsic transit time is the dominant transistor delay and parasitics such as emitter charging time are relatively small. The solid curve in Fig. 2(a) shows typical current gain $|h_{21}|$ dependence with frequency. A current gain cutoff frequency, $f_T = 244$ GHz, can be extrapolated using a -20 dB/decade roll-off [broken curve in Fig. 2(a)]. Figure 2(b) shows the dependence of f_T on ϕ_{BC}, for a fixed collector current $I_C = 31$ mA. The reduction of f_T for $\phi_{BC} < 0.9$ eV is due to the increase of collector capacitance from the forward-biased base-collector junction. For $\phi_{BC} > 0.85$ eV, the collector space-charge region is fully depleted, Z_c is constant, and the decrease of f_T arises only from an increase in τ_F. Since τ_F represents more than 60% of the total extrinsic emitter to collector signal delay, we are able to reliably calculate the transit time τ_F from the magnitude and phase of the measured s-parameter data. The error between the measured and modeled data is less than 10% as discussed in Ref. 3.

We have used Monte Carlo techniques to simulate nonequilibrium electron transport in these devices. Scattering mechanisms in the base include screened ionized impurity and the charge carrier/optical phonon excitations of the degenerate hole gas. The dominant scattering mechanisms in the collector depletion region come from optical phonons and intervalley scattering. The techniques used to calculate the appropriate scattering rates have been described previously.[4–8] The numerical methods used in our calculations are similar to those described in Ref. 7 and parameters for $In_{0.53}Ga_{0.47}As$ were taken from Ref. 8. The broken curve in Fig. 3(a) shows a calculated collector current response to a uniformly injected 3.6 ps emitter current pulse (solid curve) containing 24 000 electrons for $\phi_{BC} = 1.0$ eV. Noise in the output signal arises from the stochastic nature of the scattering processes in the base and collector.

It is apparent from Fig. 3(a) that the transistor impulse

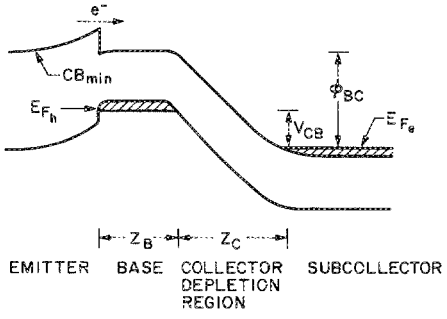

FIG. 1. Schematic band diagram of a biased N-p-n HBT. The wide band-gap InP emitter injects electrons with excess kinetic energy $E = 300$ meV into the base region of thickness Z_B. After traversing the base electrons are accelerated in the electric field of the collector depletion region. The collector-base bias is V_{CB} and the total potential drop in the collector is ϕ_{BC}. The conduction-band minimum CB_{min}, the hole Fermi energy E_{F_h}, and the electron Fermi energy E_{F_e} are indicated.

[a] Permanent address: Physics Department, University of Nottingham, England, UK.

 0003-6951/89/431789-03$01.00

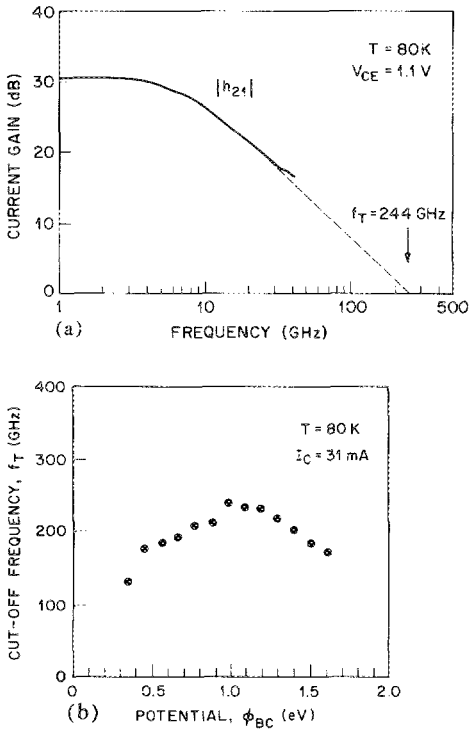

FIG. 2. (a) Solid curve shows the measured small-signal common emitter current gain $|h_{21}|$ with frequency f in the range 1–40 GHz. The transistor has an emitter area of $2.5\times11\,\mu m^2$ with a collector current $I_C = 31$ mA and collector-to-emitter bias $V_{CE} = 1.1$ V. The broken curve shows a -20 dB/decade roll-off extrapolating to a cutoff frequency $f_T = 244$ GHz. Measurements were performed with the sample maintained at a temperature of $T = 80$ K. (b) Plot of cutoff frequency f_T with total potential across the collector depletion region ϕ_{BC}. Measurements were performed with $I_C = 31$ mA and T = 80 K.

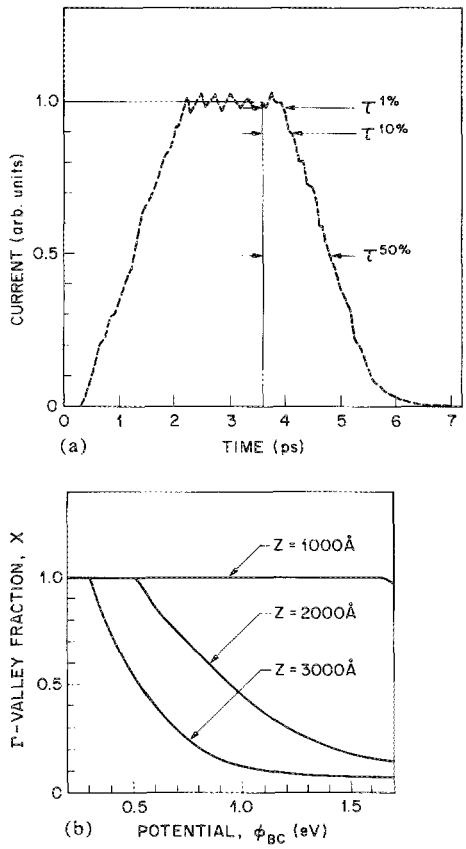

FIG. 3. (a) Numerically simulated collector current response (broken line) to a uniformly injected 3.6 ps emitter current pulse (solid line) containing 24 000 electrons with $\phi_{BC} = 1.0$ eV. Parameters used in calculation were $E = 300$ meV, $Z_B = 500$ Å, $Z_C = 3000$ Å, $p = 1\times10^{20}$ cm^{-3}, and $T = 80$ K. (b) Plot of the calculated fraction x of electrons remaining in the Γ valley for the indicated positions Z from the E-B junction as a function of ϕ_{BC} at the steady state.

response involves different delay times. This may be understood by noting that electrons which scatter into the low velocity ($v\approx2\times10^7$ cm s^{-1}) subsidiary valleys take longer to traverse the active region of the device than those electrons which remain in the high-velocity ($v\approx10^8$ cm s^{-1}) central valley. To quantify the importance of subsidiary valley transport in determining current flow through the device, we show in Fig. 3(b) a plot of the fraction, x, of electrons remaining in the Γ valley at various positions Z from the E-B junction as a function of ϕ_{BC} at steady state. For $Z = 1000$ Å, nearly all electrons remain in the Γ valley for all values of ϕ_{BC}. The significance of this is that all electrons traverse the base in the high-velocity Γ valley. For $Z = 2000$ and 3000 Å, increasing ϕ_{BC} results in a decrease in the number of electrons occupying the central valley, while the number in the low-velocity subsidiary valleys increases. Therefore, we expect the intrinsic delay τ_F to be determined by collector transport and to increase with ϕ_{BC}. This suggests that at least two delay times (τ_1 and τ_2) are required to properly describe the high-frequency response of the transistor. However, the transistor's small-signal microwave measurements are interpreted in terms of a single ensemble averaged time constant. Nevertheless, as may be seen from the experimental results shown in Fig. 4(a), this measurement technique is sensitive to the Γ-valley population. The measured increase in τ_F with ϕ_{BC} verifies the expected trend, namely, τ_F increases from 0.32 ps at $\phi_{BC} = 0.88$ eV to $\tau_F = 0.64$ ps at $\phi_{BC} = 1.6$ eV. The reason why the averaged delay time successfully models the small-signal characteristics of a device with a fraction x of injected electrons with time constant τ_1 and common base current gain α_1 in channel 1 and $(1-x)$ electrons with time constant τ_2 and current gain α_2 in channel 2 is that the difference between τ_1 and τ_2 is not very large ($\tau_2 < 3\tau_1$). Thus, when solving for the frequency ω_F at which the gain $|h_{21}| = 1$, we obtain an average delay $\tau_F = 2\pi/\omega_F$ where

$$\left|\frac{x\alpha_1 e^{-i\omega_F\tau_1} + (1-x)\alpha_2 e^{-i\omega_F\tau_2}}{1-\left[x\alpha_1 e^{-i\omega_F\tau_1} + (1-x)\alpha_2 e^{-i\omega_F\tau_2}\right]}\right| = 1, \qquad (1)$$

which quite accurately describes the response of the base and collector of the transistor and is typically sensitive to x. For large differences between τ_1 and τ_2 (e.g., $\tau_2 = 10\tau_1$), the behavior is more complicated and the use of at least two time constants in analyzing the microwave response is necessary.

We are unable to measure the large-signal response of the device at high frequency. However, results of calculating the delay time $\tau^{1\%}$, $\tau^{10\%}$, and $\tau^{50\%}$ are shown in Fig. 4(b). The delay time $\tau^{50\%}$ associated with the initial 50% fall in collector current takes longer than $\tau^{1\%}$ because a longer time is needed to collect electrons scattered into subsidiary val-

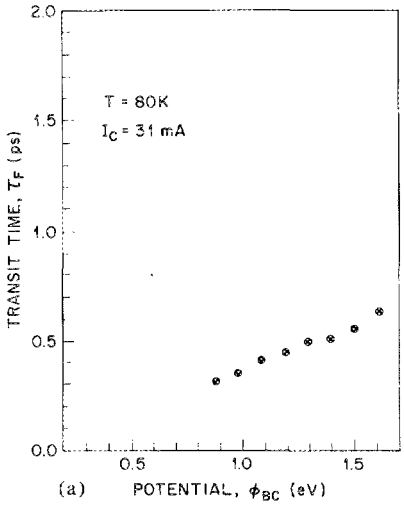

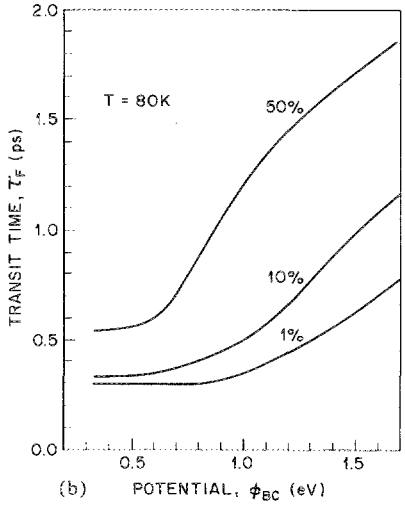

FIG. 4. (a) Plot of the measured transit delay τ_F as function of ϕ_{BC}. (b) Results of calculating $\tau^{1\%}$, $\tau^{10\%}$, and $\tau^{50\%}$ as a function of ϕ_{BC} for the parameters used in Fig. 3(a).

leys. This can be understood by observing the steady-state fraction of electrons remaining in the Γ valley near the collector contact ($Z = 3000$ Å) shown in Fig. 3(b). For $\phi_{BC} < 0.8$ eV, intervalley scattering plays an insignificant role in determining $\tau^{1\%}$. In this situation $\tau^{1\%}$ is due to extreme nonequilibrium electron transport through the structure. By way of contrast, for given ϕ_{BC}, $\tau^{50\%}$ shows a much larger delay. This is because the large signal response involves electrons which have scattered into the low velocity, low-mobility subsidiary valleys. The similarity between measured τ_F in Fig. 4(a) and calculated $\tau^{1\%}$ in Fig. 4(b) suggests that nonequilibrium central-valley transport dominates the small-signal microwave response. As a point of reference, GaAs, with its small subsidiary valley energy separation, cannot support nonequilibrium Γ-valley transport for any practical value of ϕ_{BC}.

In conclusion, we have used low-temperature microwave measurements combined with numerical simulations to study the dynamics of nonequilibrium electron transport in subpicosecond HBTs. For the first time, the influence of nonequilibrium electron transport on intrinsic device performance has been determined. The measured small-signal intrinsic transit delay τ_F increases from 0.32 to 0.63 ps with increasing collector potential drop, from $\phi_{BC} = 0.88$ to 1.6 eV, due to the increasing importance of intervalley scattering. Moreover, calculations also indicate that this scattering mechanism strongly influences the large-signal response of this device. Low collector supply voltage and small-signal swing are required to make an efficient use of nonequilibrium Γ-valley transport in compound semiconductors.

[1]K. Berthold, A. F. J. Levi, J. Walker, and R. J. Malik, Appl. Phys. Lett. **52**, 2247 (1988); **54**, 813 (1989).
[2]Y. K. Chen, R. N. Nottenburg, M. B. Panish, R. A. Hamm, and D. A. Humphrey, IEEE Electron Device Lett. **EDL-10**, 267 (1989).
[3]Y. K. Chen, R. N. Nottenburg, M. B. Panish, R. A. Hamm, and D. A. Humphrey (unpublished).
[4]M. Combescot and P. Noziers, Solid State Commun. **10**, 301 (1972).
[5]A. F. J. Levi and Y. Yafet, Appl. Phys. Lett. **51**, 42 (1987).
[6]W. Bardyszewski and D. Yevick, Appl. Phys. Lett. **54**, 837 (1989).
[7]P. H. Beton and A. F. J. Levi, Appl. Phys. Lett. **55**, 250 (1989).
[8]L. W. Massengill, T. H. Glisson, J. R. Hauser, and M. A. Littlejohn, Solid-State Electron. **29**, 725 (1986).